Materials Today Communications 35 (2023) 106294

Contents lists available at ScienceDirect

Materials Today Communications

journal homepage: www.elsevier.com/locate/mtcomm

Analysis of the applicability and state monitoring of material extrusion–printed acrylonitrile butadiene styrene injection mould inserts with different infill levels

Szabolcs Krizsma [a], András Suplicz [a,b,*]

[a] Department of Polymer Engineering, Faculty of Mechanical Engineering, Budapest University of Technology and Economics, Műegyetem rkp. 3., H-1111 Budapest, Hungary
[b] MTA-BME Lendület Lightweight Polymer Composites Research Group, Műegyetem rkp. 3., H-1111 Budapest, Hungary

ARTICLE INFO

Keywords:
Rapid prototyping
Rapid tooling
Injection moulding
Deformation measurement
Material Extrusion

ABSTRACT

The widespread appearance of additive manufacturing (AM) proved to be a game changer for many traditional plastic processing technologies in the last few years. The application of AM for injection mould making has become a new and promising direction of rapid tooling (RT), especially with the emerging demand for more customizable products. A possible solution to satisfy the desire for mass customization is the application of additively manufactured low-volume moulds and inserts. These prototype moulds also give an excellent opportunity to check and validate designs in a real-life operational environment, before the expensive large-volume steel mould is made. Material extrusion printing was used to produce injection mould inserts from acrylonitrile butadiene styrene (ABS). These inserts proved to be suitable for low-volume injection moulding. The inserts were printed with different infill levels: 80 %, 50 % and 25 %. In previous articles, an earlier unknown complex state monitoring method was created to analyse and quantify in-mould operational behaviour of additively manufactured injection mould inserts. In the present article, this measurement system was applied to material extrusion–printed prototype moulds. This system measures strains (at two locations) and the temperature distribution of the inserts (both volumetric temperature and cavity surface temperature). 3D scanning and conventional thickness and mass measurements were also applied to characterize the dimensional accuracy of the injection moulded products and the inserts as well. The correlation between the definite integral of measured operational strains (occurring during the injection moulding cycles, from the start of holding to the end of the holding phase) and the resulting product properties (mass and thicknesses) was also analysed. An excellent linear correlation was found between them (mostly $R^2 > 0.9$). This finding can pave the way for a more automated quality control system because of its practical applicability and relative ease of use.

1. Introduction

The combination of additive manufacturing and conventional injection moulding is an excellent new way to mass-produce customized products. Rapid-prototyped moulds also provide an outstanding opportunity to run injection moulding trials before the expensive large-volume steel mould is made, as it was discussed by [1]. The international research community has started to analyse the applicability of rapid tooling, therefore several case studies are already available [2,3]. Yet, this area still has a long way to go before its full potential can be realised. Researchers have not measured the operational deformations and the thermal state of injection moulds simultaneously, especially in the case of additively manufactured, low-volume moulds. Only a handful of studies are available on the comprehensive state monitoring of injection moulds [4].

Additive technologies have already made their way into mould making. Laser powder bed fusion (LBPF) can make metal mould inserts that can be used for high-volume production. Koker et al. [5] proved that metal printing allows the production of complex geometries, like coextrusion dies, reducing the need for conventional machining. Additive technologies also make feasible the much desired freeform geometries including conformal cooling channels and lattice structures that increase

* Corresponding author at: Department of Polymer Engineering, Faculty of Mechanical Engineering, Budapest University of Technology and Economics, Műegyetem rkp. 3., H-1111 Budapest, Hungary.
E-mail address: suplicz@pt.bme.hu (A. Suplicz).

https://doi.org/10.1016/j.mtcomm.2023.106294
Received 13 April 2023; Received in revised form 19 May 2023; Accepted 23 May 2023
Available online 24 May 2023

cooling efficiency and enhance productivity. Chantzis et al. [6] improved the cooling performance of hot stamping dies using lattice structures. Muvunzi et al. [7] applied conformal cooling to enhance the efficiency of a hot stamping die. Kuo et al. [8] analysed the effect of different conformal cooling channels on the injection moulded product. Török et al. [9] applied the combination of conformal cooling and a multi-material mould insert (3D printed shell cast with copper) to further reduce residual cooling time in injection moulding. The optimization of the internal cellular structure results in better heat extraction, acceptable mechanical strength and a significant weight reduction of injection moulds. Park et al. [10] used a titanium alloy to print an injection mould and optimised the shape of the applied lattice structure. Mahshid et al. [11] also reached promising results by applying compression tests and simulation to determine the strength of lattice structures applicable in mould components. Narvan et al. [12] highlighted that metal printing also faces challenges (like residual stresses and part deflection after printing), which need to be met.

Polymeric moulds are gaining ground in low-volume production and individual prototype making. Non-thermoplastic resins processed by material jetting (MJ) (typically by PolyJet technology) or vat photopolymerization are suitable for making such prototype injection moulds. These moulds are inferior to steel moulds in terms of mechanical strength and thermal resistance but they can adequately produce small product volumes. Shan et al. [13] proved that non-thermoplastic polymer parts are capable of shape memory that can also enhance product dimensional accuracy. Bagalkot et al. [14] PolyJet printed injection mould inserts and created an algorithm to set process parameters in order to maximize insert life expectancy. They reached 54 cycles with their DigitalABS test mould. Giorleo et al. [15] also made IM mould inserts from a high-temperature resin by MJ. They proved that printing orientation has a significant effect on the operational behaviour of the inserts and that the inserts are suitable for micro injection moulding. Zink et al. [16] experimented with different cooling channel layouts for PolyJet printed mould inserts and found that conformal cooling can decrease the heat load of the inserts by almost 70 % and therefore increase mould life expectancy. Alongside material jetting, the vat photopolymerization technique is also a popular choice for low-volume mould making. Walsh et al. [17] created a grading system including the analysis of the flexural modulus, the thermal conductivity and the dimensional accuracy of specimens printed by stereolitography from various resins to determine the suitability of the materials for injection mould making. Walsh et al. [18] proved that stereolitography-printed prototype moulds can be used to customize product geometries, which provides a new research direction for high-end applications like the injection moulding of pharmaceutical tablets.

Some case studies focus on the comparison of conventionally and additively manufactured moulds. Hopkins et al. [19] compared three SLA-printed moulds and a conventional steel mould. The two SLA moulds endured more than 50 cycles and the third one failed after 20 cycles. Mendible et al. [20] compared machined mould inserts, a DMLS-printed insert and a PolyJet-printed insert. Metal inserts were used for 500 injection moulding cycles without any visible damage while the PolyJet insert cracked after 116 cycles.

Researchers also experiment with thermoplastic polymer patterns and moulds. Arias et al. [21] optimised material extrusion printer hotends to achieve better printing quality of thermoplastic polymer parts and to enhance printing speed. Choe et al. [22] printed patterns for investment casting a complex geometry (a centrifugal compressor impeller). They proved that thermoplastic polymer filaments processed by material extrusion (ME) are especially practical for such tasks. Gohn et al. [23] applied ME for injection mould making and successfully produced a low-volume mould. Park et al. [24] experimented with advanced ME printers that even allow researchers to make parts from the highest quality thermoplastic polymers like polyetheretherketone (PEEK). Research articles are also available on the ME printing of metal injection moulding feedstock. Singh et al. [25] proved that polymer-coated metal particles can be printed with special ME printers, then the so-called green part can be debinded and sintered at high temperature to remove the polymer coating. Seleznev et al. [26] also ME printed metal parts (including conformally cooled mould inserts) with an arbitrary infill structure inside them that they later infiltrated by another metal; this way, the properties of the two metals are combined. Another emerging area of ME is the printing of carbon fibre–reinforced polymer composites. These are especially suitable for moulds, due to their increased mechanical strength and thermal conductivity. Yeole et al. [27] proved that the thermal conductivity of the carbon fibre–reinforced polymer composite mould can be influenced by the applied infill pattern. The variability of the infill level for ME printing is also desirable in pharmaceutical applications. Fuenmayor et al. [28] manufactured tablets by the combination of different infill level ME printing and injection moulding that allows the mass customization of medicine. Sacrificial moulds can also be printed by ME, which gives large product design freedom. Wick-Joliat et al. [29] proved that these sacrificial moulds can even be used for ceramic injection moulding. Studies are also available on the dimensional accuracy of different thermoplastic polymer printing technologies. Minetola et al. [30] showed that the accuracy of material extrusion is highly dependent on minimal layer thickness, while powder-based sintering processes are influenced by minimal powder particle size.

As a conclusion, it can be stated that additive technologies have already made their mark on conventional mould making. Material extrusion is a popular, widespread and dynamically developing branch of additive manufacturing, which has high potential in mould making. Even though the benefits are self-evident, the area is scarcely researched and many articles focus solely on feasibility checks and injection moulding trials. On the other hand, the comprehensive state monitoring, presented in [1] and [4] is largely unknown in the rapid tooling world. Such measurement system allows the quantification of injection moulding process parameters like operational strains and temperature distribution (both volumetric and cavity surface temperatures). This work fills a knowledge gap and adds to the already existing knowledge base because it allows a more exact and numeric understanding of the operational behaviour of prototype moulds. This work also offers direct comparability and benchmarking, since the presented comprehensive state monitoring method can be applied to injection moulds manufactured by numerous different additive and conventional technologies. In the present article, injection mould inserts were printed with three different infill levels: 80 %, 50 % and 25 %, and injection moulding tests were run with them. The operational strains, surface temperature and volumetric temperature of the inserts were measured. The dimensional accuracy of the products was also analysed using 3D scanning, and conventional mass and thickness measurement. Correlational diagrams were set up between measured strains, and product masses and thicknesses and excellent correlations were found between them. These correlations can later be used for real-time product quality control.

2. Materials and methods

2.1. The comprehensive state monitoring method

The goal of the present study is to numerically specify the main injection moulding process parameters, including the operational strain of mould inserts at two locations, operational cavity surface temperature and temperature at the back of the inserts. Two strain gauges (KMT-LIAS-06-3-350-5EL) measured strains both at the near gate (NG) and the far from the gate (FFG) locations and a Spider 8 unit (Hottinger Baldwin Messtechnik GmbH) collected their data. The strain gauges were glued into their slots with a cyanoacrylate adhesive: 3 M Scotch Weld Plastic and Rubber Instant Adhesive PR100. The temperature at the back of the insert was measured by a Heraeus M222 Pt100 thermocouple and an Ahlborn Almemo 8990–6 unit collected its data. The thermocouple was also glued with the previously mentioned cyanoacrylate adhesive. Fig. 1

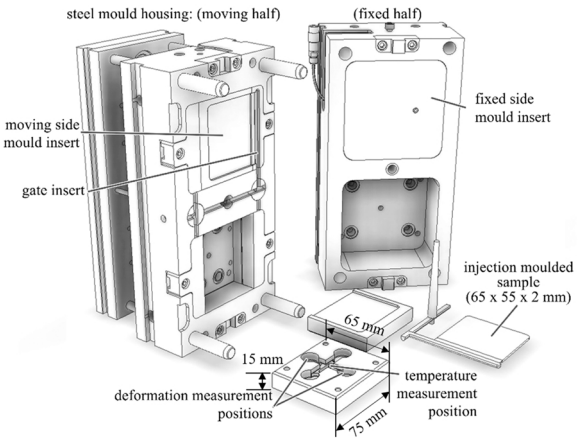

Fig. 1. The complete test mould, the moving side insert and the injection moulded product.

shows the test mould, the moving side mould insert, as well as the locations of the strain gauges and the thermocouple. Only the upper cavity was used for the injection mouldings, so a cylindrical runner insert shut off the lower cavity. The injection moulded product was a plate with the overall dimensions of 65 × 55 × 2 mm and the cavity was filled through an edge gate (1 mm thick).

2.2. Producing the mould insert

The mould inserts were 3D printed using a CraftBot Plus material extrusion printer (CraftUnique Kft). The printed material was an Acrylonitrile Butadiene Styrene: Z-ABS (Zortrax S.A.) (with its relevant properties in Table 1). This material grade has acceptable mechanical properties and suitably high glass transition temperature for prototype injection mould making.

The varying parameter was infill percentage. The three analysed levels were 80 %, 50 % and 25 %. Infill percentage was chosen as the varying parameter because it fundamentally influences both the insert printing time and the stiffness. The fill pattern was selected to be grid. Filament diameter was 1.75 mm, printer bed temperature was 100 °C and extruder temperature was 250 °C. The printing layer height was 0.2 mm and the nozzle diameter was 0.4 mm. The resulting printing times for the mould inserts were 4 h 1 min (at 80 % infill), 3 h 23 min (at 50 % infill) and 2 h 48 min (at 25 % infill). Fig. 2 shows the different infill levels. The supporting infill structure inside the slots of the strain gauges and the thermocouple was removed after printing.

The fixed-side mould insert was made of EN AW 5754 general-purpose aluminium, which has three orders of magnitude higher thermal conductivity than ABS (147 W/(m K) compared to ~0.1–0.2 W/(m K)).

2.3. The injection moulding of samples

The injection moulded material was Tipplen H145F polypropylene homopolymer (MOL Group PLC.). It is ideal because of its excellent MFR value (29 g/10 min at 230 °C and 2.16 kg), low recommended processing temperature range (190–235 °C) and incompatibility with ABS.

The injection moulding machine was an Arburg Allrounder Advance 270 S 400–170 (ARBURG GmbH) with a screw diameter of 30 mm. Clamping force was 5 tons, the injection rate was 15 cm^3/s, the injection pressure limit was 500 bar, holding time was 15 s, residual cooling time was 30 s and dose volume was 40 cm^3. To protect the inserts from excessive heat, delay times were kept between the cycles. The overall cycle time was 300 s from which the injection moulding cycle from mould closing to mould opening was approximately 56.6 s. The rest was the idle time in the open state of the mould. First, a mould filling test was made to find the switchover point. Switchover volume was initially set to 35 cm^3 and it was decreased in 2 cm^3 steps to reach complete filling. Optimal switchover volume was found at 25.5 or 26 cm^3 depending on the thermal expansion of the mould inserts.

Table 1
Material properties of Z-ABS.

Physical properties	Unit	Typical value
Tensile strength	MPa	30.46
Breaking stress	MPa	25.89
Elongation at max tensile stress	%	4.52
Elongation at break	%	11.08
Flexural modulus	GPa	1.08
Glass transition temperature	°C	107.89
Shore hardness (D scale)	–	69.2

3. Results and discussion

3.1. Printing quality analysis of the mould inserts

The newly printed moving side inserts were 3D scanned before the injection moulding series. 3D scanning highlights production tolerances and warpage at the outer corners of the parts. Scanning was done by a GOM ATOS Core 5 M scanner (GOM GmbH). Warpage at the corner points reached 0.5–0.6 mm, while most of the back surface remains nearly at the nominal dimension. The nominal thickness of the insert is 15 mm, which means that the size deviation is 3–4 %. Warpage occurs mostly in the corners of the insert, where the printed material can easily detach from the printer bed, due to the more intense cooling. It is similar for the cavity surface, where the corners of the plate show higher than nominal dimensions and the centre is dimensionally accurate. This inevitably influences the quality of the injection moulded product. Due to the presence of warpage, the proper orientation of the part and careful choice of building direction is essential. Surfaces of the insert that form the parting plane should have minimal warpage and acceptable planarity for proper mould closing and to avoid flash. It is also important that the overall dimensions of the insert are lower than nominal (by approximately 0.19–0.35 mm), which can result in flash between the inserts and the mould housing. Therefore, part shrinkage should also be taken into consideration and compensated for when the insert is designed. The required scaling factor (the part is designed to be larger by this factor) to compensate for shrinkage can be determined by printing trials, and prior experiences. Another important observation is that the quality of the cavity surface is not perfect because the remnants of the filaments are present. The reduction of printing speed or the increase of melt temperature can enhance the quality of the cavity surface.

3.2. Insert deformation during operation

3.2.1. Injection moulding series: constant injection moulding parameters

After finding the proper switchover points, injection moulding series were run with the three inserts. Operational strains (occurring during the injection moulding cycles) were measured and then plotted as a function of time. Absolute strain results are presented in Fig. 3 for the three inserts. The insert with 80 % infill (Fig. 3a) shows excellent reproducibility because strain curves remain almost identical cycle to cycle. Maximal strains vary between 0.15 % and 0.17 % in the 2nd to 10th cycles. The NG strains necessarily exceed the FFG strains because the melt pressure drops along the flow length and the heat transfer from the melt to the insert also greatly depends on local cavity pressure. As infill was decreased to 50 % and 25 %, the measured absolute strains grew significantly: maximal strains were in the range of 0.23–0.3 % in the case of 50 % infill and 0.2–0.26 % in the case of 25 % infill. This increase in strain is the direct result of the inevitable loss of insert stiffness. The shape of the strain curves also tend to vary cycle to cycle especially in the case of the 25 % infill insert. A clear change can be seen from the 7th

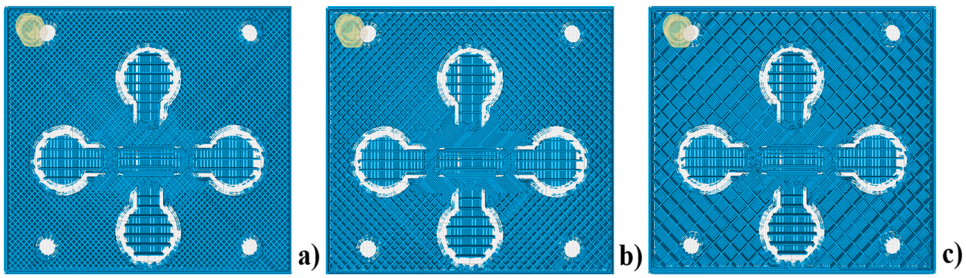

Fig. 2. Material Extrusion printed mould inserts at 80 %, 50 % and 25 % infill levels (a, b and c), respectively.

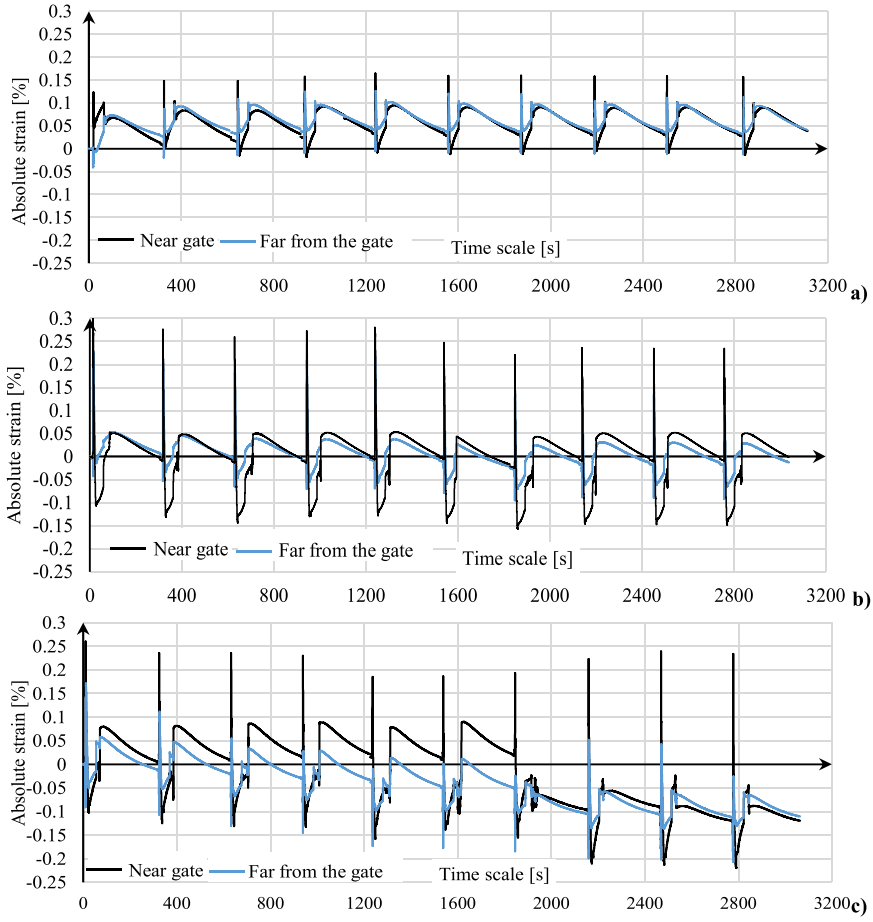

Fig. 3. Absolute strain results at a constant 75-bar holding pressure for 80 % infill a), 50 % infill b) and 25 % infill c).

cycle on (25 % infill), which can be the result of irreversible mechanical damage to the insert. Fluctuations in the shape of the strain curves at constant injection moulding parameters indicate deteriorating reproducibility as the value of insert infill drops. The shape of the strain curves also changes because steeper drops can be observed in the strain at part ejection at the lower infill levels. This is caused by flash between the cavity insert and the edge gate insert (indicated in Fig. 1).

Fig. 4 presents the graphical explanation of the injection moulding cycle elements on the absolute strain–time curve. The first spike at the absolute strain–time curve corresponds to the maximum strain occurring approximately at the end of the filling phase. After that maximum point, a downturn can be seen in the absolute strain in the first half of the holding phase. This decrease is caused by the loss in injection pressure, occurring at the switchover point. In the second half of holding and in the residual cooling time, absolute strain gradually increases as the heat is slowly extracted from the injection moulded product towards the

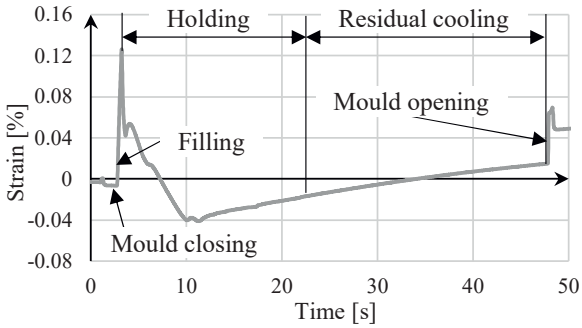

Fig. 4. Injection moulding cycle elements on the absolute strain-time curve.

mould insert. The stiffness of the heated insert decreases and thermal expansion occurs. The third factor, causing the increase of strain, is the viscoelastic behaviour of ABS, as it tends to creep, especially at higher temperatures. After the residual cooling time, the mould opens and the part is ejected. At this point, the clamping force and the pressed-in product no longer deforms the insert. The steep strain increase at mould opening indicates that the cavity is slightly overfilled. The cavity is suddenly unloaded as the part is ejected and from that point on, the mould insert can expand freely out of the parting plane. Thermal expansion occurs largely in the idle time between the cycles. It is caused by the low thermal conductivity of the polymer mould material and the presence of heat-insulating air inside the insert, due to the infill structure.

Reproducibility of the injection moulding cycles can be well characterised by the relative strain-time curves that are presented for the three infill levels in Fig. 5. Relative strain quantifies the change in strain within a single injection moulding cycle. It can be expressed as follows:

$$\varepsilon_{rel,i}\,(t) = \varepsilon_{abs,i}(t) - \varepsilon_{res,i-1} \quad (1)$$

where $\varepsilon_{rel,i}(t)$ is the relative strain in the i^{th} cycle, $\varepsilon_{abs,i}(t)$ is the absolute (measured) strain in the i^{th} cycle and $\varepsilon_{res,i-1}$ is the residual strain from the $(i-1)^{th}$ cycle. The concept of relative strain was already discussed in [1].

At 80 % infill (Fig. 5a), the maximal relative strain values are around 0.13 % and they can be measured almost instantaneously at complete filling. From the switchover point on, the relative strain decreases in the holding phase (due to the previously mentioned injection pressure loss) and only a minor increase can be observed in the residual cooling time caused by the delayed heat transfer from the injection moulded product. Heating of the insert results in the thermal expansion, creep and loss of stiffness of the insert material. At mould opening and part ejection, a minor, stepwise increase can be found in relative strain, due to the disappearance of the clamping force. The 1st and the 2nd cycles are basically setup cycles, where the pressure load and thermal expansion push the insert into its final position. From the 3rd cycle on, the relative strain curves are almost identical, showing an excellent reproducibility of the technology. The shape of the relative strain–time curves are similar in the case of the 50 % and 25 % infill levels (Fig. 5b and c, respectively), but maximal relative strain values vary between 0.24 % and 0.3 % in the case of 50 % infill and fluctuate above 0.3 % in the case of 25 % infill. Significantly lower relative strains occur in the second part of the holding phase and in the residual cooling time compared to the 80 % infill insert. The stepwise increase at part ejection is also higher for the 50 % and 25 % infill inserts, which indicates that the cavity is more overfilled than in the case of the 80 % infill insert. It is also worth noting that relative strain curves show higher divergence at the 50 % and the 25 % infill levels, which also indicates deteriorating reproducibility of the injection moulding cycles at lower infill levels.

3.2.2. *Injection moulding series: increasing holding pressure*

As was discussed earlier, decreasing the infill results in steeply increasing strains both at NG and FFG locations. After injection moulding 10 cycles at a constant 75-bar holding pressure, holding pressure was increased from 50 bar in 25-bar steps in every second cycle. Fig. 6 presents the effect of increasing holding pressure on operational strains. At 80 % infill (Fig. 6a), the absolute strain curves show excellent repeatability up to a holding pressure of 175 bar. From that level on, both maximal strains and residual strains increased, indicating the gradual deformation of the insert. At a holding pressure of 275 bar, the melt punctured the surface of the cavity. The insert with 80 % infill endured 32 operational cycles (with holding pressure applied). At 50 % infill (Fig. 6b), the NG gauge signal started failing at a holding pressure of 125 bar, and after that level, there was a sharp increase both in the NG and FFG strains. At a holding pressure of 200 bar, the NG gauge ruptured, leading to questionable further results. The FFG strain gauge provided acceptable results up to a holding pressure of 200 bar. The 50 % infill insert endured 31 operational cycles with holding pressure. At 25 % infill (Fig. 6c), the measurement of strain failed at the holding pressure of 175 bar. Failure of the NG and FFG gauges happened almost simultaneously. The melt pierced the mould insert at the holding pressure of 225 bar. The insert endured 24 operational cycles with holding pressure.

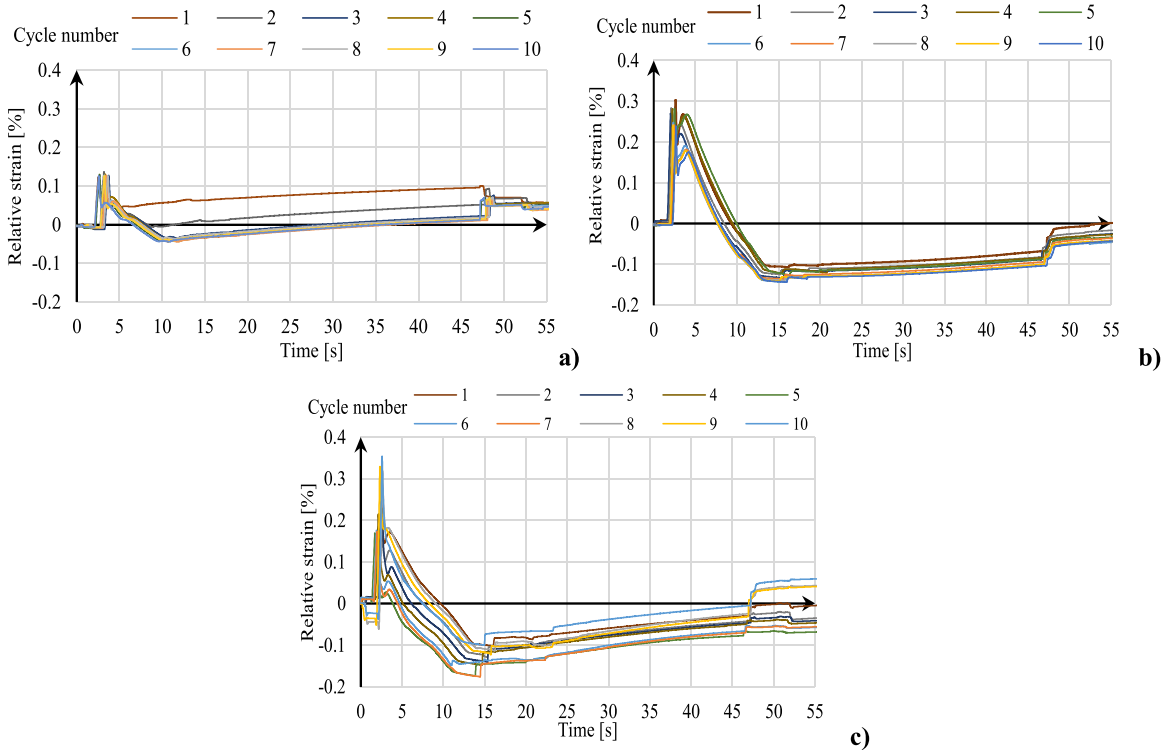

Fig. 5. Relative strain–time curves at a constant 75-bar holding pressure for 80 % infill a), 50 % infill b) and 25 % infill c).

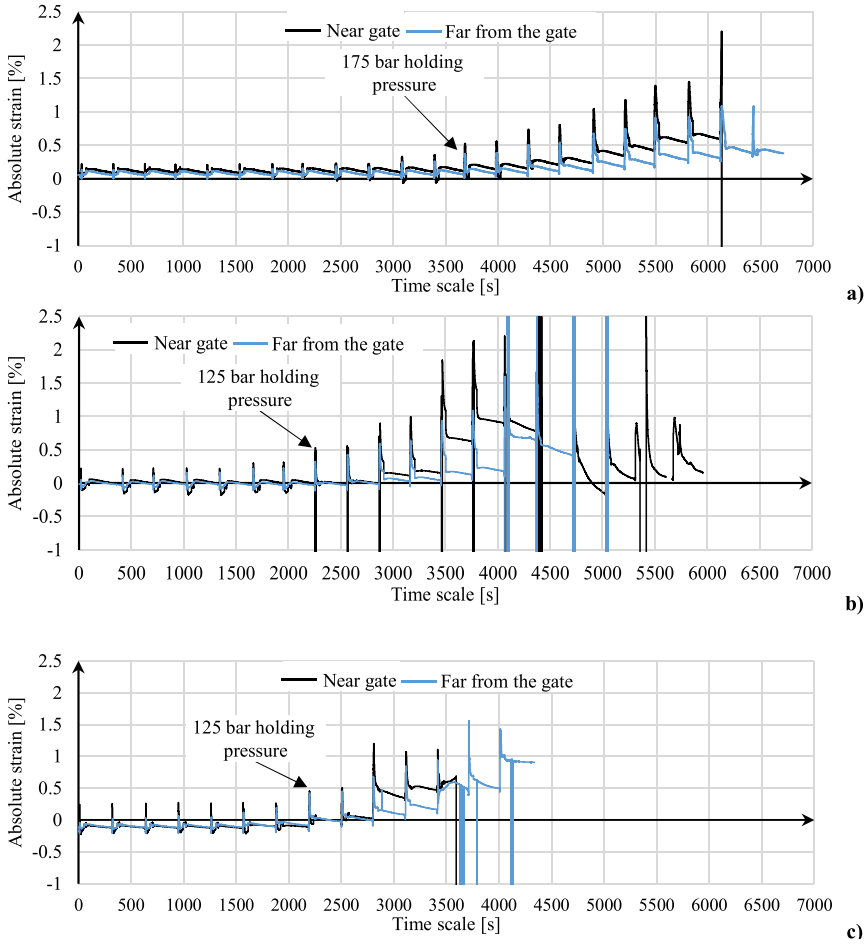

Fig. 6. Absolute strain results of the increasing holding pressure section of the injection moulding series for 80 % infill a), 50 % infill b) and 25 % infill c).

These results indicate that as infill level decreases, so do the maximal reachable cycle numbers. All three measurement series show that the NG strains exceeded the FFG strains. In addition, the operation of the strain measurement system becomes more unstable at lower infill due to the increased deformations. The NG strain gauges fail earlier than the FFG gauges. It is also clear that as holding pressure increased, the difference in the NG and FFG strains grew steadily. It is probably caused by the pressure drop along the flow length and the pressure dependence of the local heat transfer from the product to the mould. The NG location is subjected to a higher pressure load and therefore a higher thermal load.

The combined effect of decreasing infill and increasing holding pressure is also shown in the relative strain–time curves. Fig. 7 presents the relative strain curves measured at the NG location at different holding pressures. The maximal relative strains increase significantly with increasing holding pressure at all three analysed infill levels. At 80 % infill, the maximal relative strain grew from 0.11 % at a holding pressure of 50 bar to 0.97 % at 250 bar, which is an almost ninefold increase. At 50 % infill, relative strain was 0.22 % at 50 bar, which rose to 0.88 % at a holding pressure of 175 bar. As Fig. 7b) shows, strain measurement did not provide data about the maximum of the relative strain curves at higher holding pressures (200 and 250 bar) as the strains exceeded the measurement range of the gauge. At 25 % infill, maximal

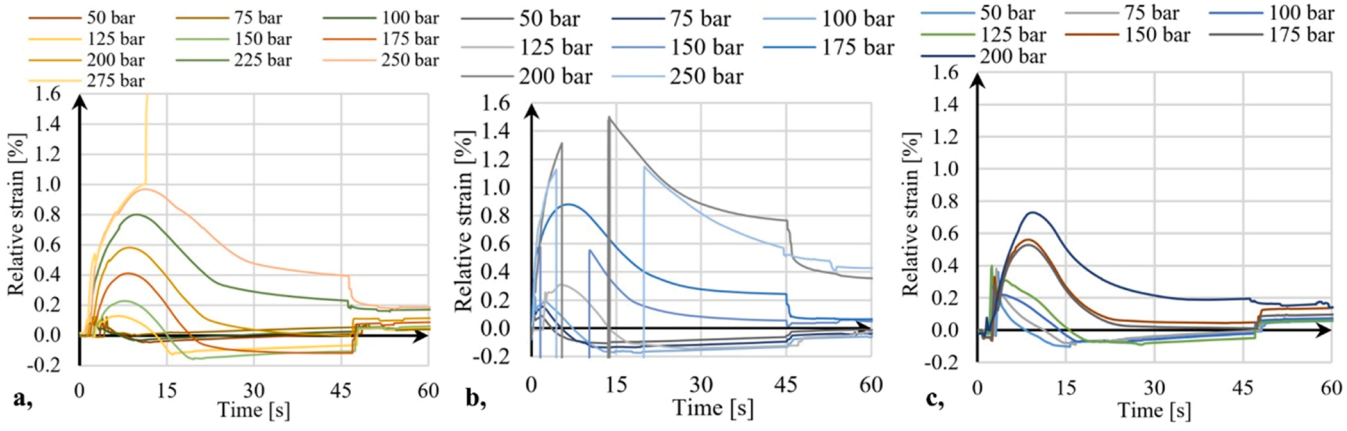

Fig. 7. Relative strain results at the NG location at different holding pressures. 80 % infill a), 50 % infill b) and 25 % infill c).

relative strain at a holding pressure of 50 bar was already 0.35 %, which climbed to 0.75 % at 200 bars.

As holding pressures were increased, relative strains also stabilised at higher levels in the holding and residual cooling phases. At 80 % infill (Fig. 7a) the relative strains at mould opening grew from − 0.1 % at 50 bar (indicating a slight compression of the gauge) to 0.4 % at 250 bar. At 50 % infill (Fig. 7b), relative strain at 50 bar was − 0.12 % at mould opening, which grew to 0.52 % at 250 bar. The strain increased because the growing holding pressure gradually overfilled the cavity. Overfilling is also enhanced by the low cooling speed and the slower freeze of the injection moulded product, due to the bad thermal conductivity of the polymeric mould insert.

3.3. The temperature of the inserts

Thermocouple temperature measurements provide data about the volumetric temperature of the insert. Fig. 8 shows these results for the three different infill levels. Volumetric temperatures oscillate as the injection moulding cycles occur, but the overall tendency is clearly increasing. At lower infill levels, volumetric temperature grows at a faster pace because the volume fraction of air (acting as a heat insulator) increases. The temperature at the back of the inserts climbed from room temperature at the beginning of the injection moulding series to above 40 °C by the start of the last cycles. Effective insert temperature at the back can be even higher than the measured temperatures. All of the inserts failed when the melt punctured the cavity above the slots of the strain gauges and filled the slots at the back of the inserts. This failure caused the spikes at the end of the curves in the last cycles, which show the temperature of the injected melt.

Thermal imaging camera was also applied to determine the cavity surface temperature of the moving side mould insert in the idle time between the cycles. These results are presented in Fig. 9 for the three inserts. Each temperature–time curve in these diagrams corresponds to the cooling of the centre point of the cavity in the idle time between two cycles (~250 s each). The tendency is similar to the thermocouple results because the lower infill level leads to faster heating of the mould as well as higher maximal surface temperatures upon mould opening. In the case of the 80 % infill insert (Fig. 9a), heating of the insert is more gradual, and surface temperature only exceeded 80 °C in the 31st cycle. However, in the case of the 50 % infill (Fig. 9b), surface temperature rose above 80 °C in the 26th cycle and it even surpassed 100 °C by the time of failure (31st cycle). Such a high value is in the region of the glass transition temperature, where the stiffness and strength of the insert decrease considerably. The combination of the thermocouple and the thermal imaging camera measurements gives a comprehensive view of the thermal state of the polymeric mould inserts. This way, the mould inserts can be protected from excessive heat loads and their life expectancy can be increased.

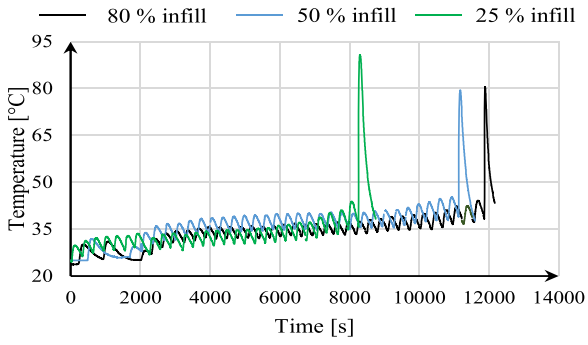

Fig. 8. Thermocouple temperature measurement results at different infill levels.

3.4. Analysis of product quality

Product mass and product thickness were also measured at two locations: above the NG and FFG slots. In the constant holding pressure section (1st to 10th cycles), both product mass and thickness remained relatively constant. For the 80 % infill insert, the weight of the 1st plate was 5.72 g, which remained at 5.70 g in the 10th cycle. For the 50 % infill insert, product weights were 5.45 g in the 1st cycle and 5.43 g in the 10th cycle. For the 25 % infill insert, product weight was 5.60 g in the 1st cycle and it was 5.67 g in the 10th cycle. Plate thicknesses show a similar tendency in the constant holding pressure section. For the 80 % infill insert, maximal plate thickness (measured in the NG location) was 1.925 mm in the 9th cycle, while minimal thickness was 1.85 mm in the 10th cycle. For the 50 % infill insert, these values were 1.758 mm in the 9th cycle and 1.872 mm in the 10th cycle. For the 25 % infill insert, minimal product thickness was 1.835 mm in the 7th cycle and maximal thickness was 1.946 mm in the 1st cycle. These small deviations are well within the range of the uncertainty of switchover, especially for a hydraulic injection moulding machine. However, as higher holding pressures were applied, plate thickness and mass increased steadily. A lower infill level results in steeply increasing product mass and thickness even at lower holding pressure levels. The conclusion is that product properties are heavily dependent on the applied holding pressure and the level of infill (Fig. 10, Table 2).

3.5. Warpage and shape distortion of the injection moulded products

The fixed side mould insert (made from EN AW 5754 general-purpose aluminium) extracts significantly more heat than the moving side insert, made from ABS. This results in the warpage of the injection moulded plates. The cavity surface layers of the printed inserts also lose stiffness due to the excessive heat load from the injected melt. This softened upper surface layer is pressed upon the infill structure beneath. This can be best observed in the case of the lowest, 25 % infill insert, especially on the last few products where surface temperature and the applied holding pressures were both high. Fig. 11 shows the 3D scanned images of the products. These 3D scanning results also highlight the local shape distortions above the locations of the insert failure as well as the warpage of the plates.

3.6. Failure mechanism of the inserts

After the injection moulding series, the mould was disassembled and the failed inserts were 3D scanned. These results are presented in Fig. 12. Excessive residual deformation can be found on the inserts above the slots for the strain gauges because of the locally decreased wall thickness. Due to the thermoplastic insert material, these deformations do not completely recover. The inserts failed when the melt pierced the cavity at a strain gauge slot and filled the grooves at the back of the inserts. In the case of the 50 % and 25 % infill inserts, the imprint of the internal infill structure is also clearly visible on the cavity surface. As the infill structure becomes less dense, it cannot properly transfer the pressure load from the cavity surface, which causes the closing layers (forming the cavity surface) to be pressed into the insert. The closing layers of the 50 % and 25 % infill inserts were also damaged along the edge gate, which made part ejection difficult because flash occurred between the edge gate insert and the cavity insert. The cavity surface of the 25 % infill insert was heavily damaged, as deep distortions can be seen covering large portions of the cavity surface area. These deformed areas are concentrated around the edge gate as the pressure and temperature load is higher there compared to the end of the flow length.

3.7. Correlations between strain and product quality

The strain integral was introduced as a scalar quantity, which was correlated with product thickness and product mass. The definite

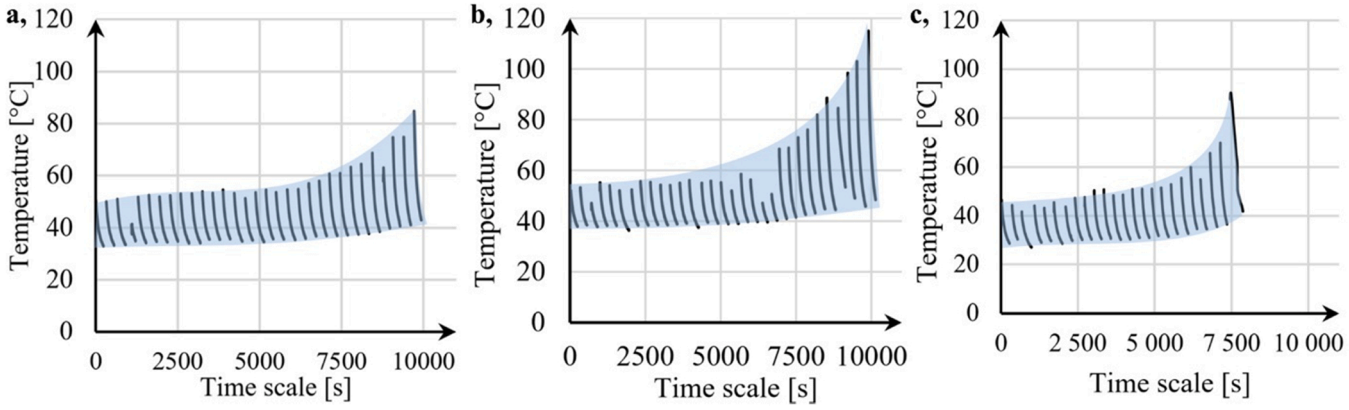

Fig. 9. Cavity surface temperature of the mould inserts, measured with a thermal imaging camera. 80 % infill a), 50 % infill b) and 25 % infill c).

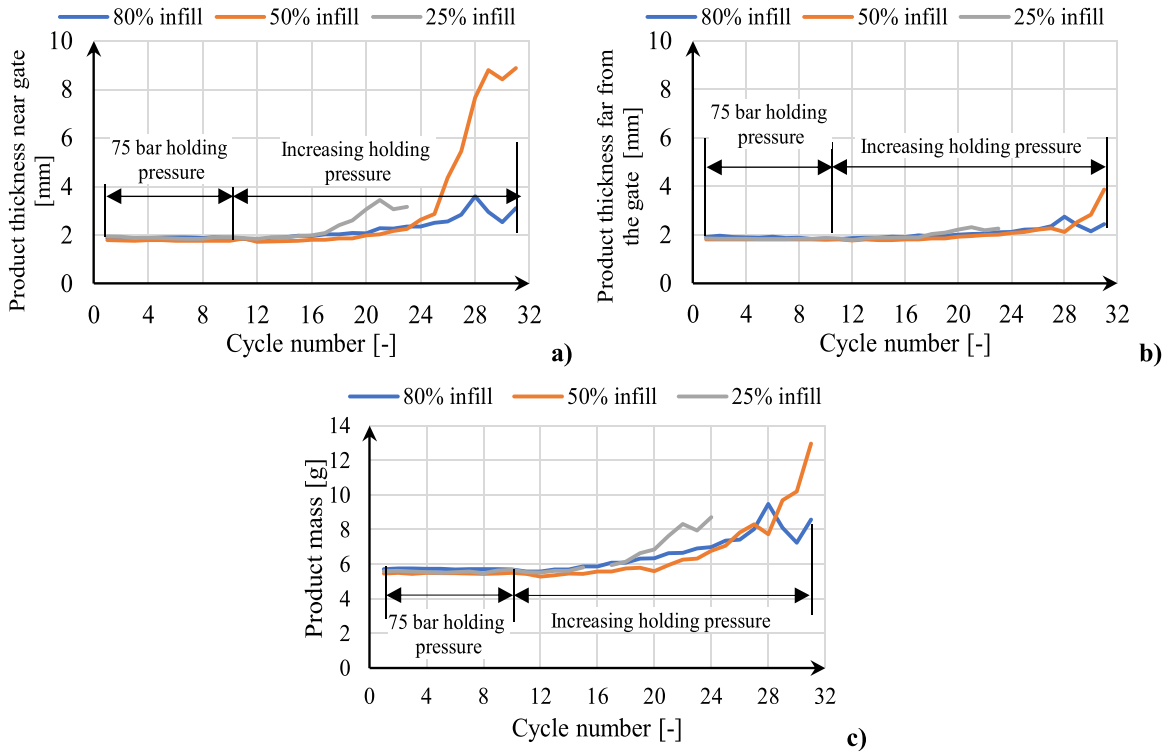

Fig. 10. NG product thickness a), FFG product thickness b) and product mass c), of the plates made by the three different inserts.

Table 2
Average product mass and thickness of the plates injection moulded at 75 bars constant holding pressure with the three different infill level inserts.

Infill	Mass & standard deviation [g]	Thickness NG & standard deviation [mm]	Thickness FFG & standard deviation [mm]
80 %	5.724 ± 0.017	1.887 ± 0.021	1.890 ± 0.036
50 %	5.464 ± 0.023	1.781 ± 0.012	1.812 ± 0.010
25 %	5.571 ± 0.061	1.890 ± 0.038	1.842 ± 0.012

integrals of the absolute strain–time curves were calculated from the beginning of holding to the end of the holding phase. These calculations were made for each cycle, both at the NG and at the FFG locations, for all three inserts. Then the measured product masses and thicknesses were correlated with the calculated strain integral values. Absolute strain is suitable to take into account the cycle-to-cycle accumulation of strains (already presented in Fig. 6). The time boundaries of the definite integral was chosen from the start of the holding to the end of the holding phase because that is the time window when additional material is injected into the cavity for shrinkage compensation (Fig. 13).

A linear equation was fitted to the corresponding absolute strain integral and product mass/thickness values, and strong correlational coefficients were found (both mass and thickness). Diagrams for the absolute strain integral–product mass data are shown in Fig. 14. Good correlations were found for all three infill levels. Therefore, a strong linear relation can be assumed between the absolute strain integrals and product mass (mostly $R^2 > 0.9$).

Similarly to product mass, product thickness also shows strong correlation with the absolute strain integral (Fig. 15). NG strains were correlated with NG product thickness and the FFG strain integrals with FFG thicknesses. Correlational coefficients also exceeded $R^2 > 0.9$ in nearly all the analysed cases, reinforcing that the measurement of strain is a suitable product quality monitoring tool.

The results presented in Figs. 14 and 15 can be expressed mathematically by Eqs. (2) and (3) for product mass and thickness,

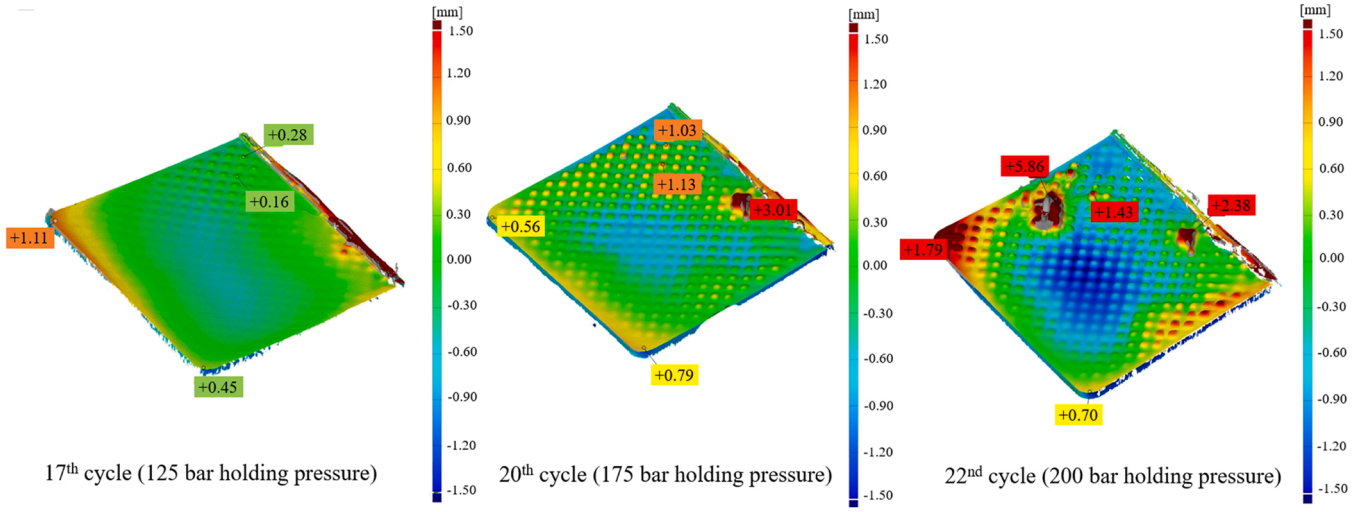

Fig. 11. 3D scanned images of the injection moulded products, made with the 25 % infill insert.

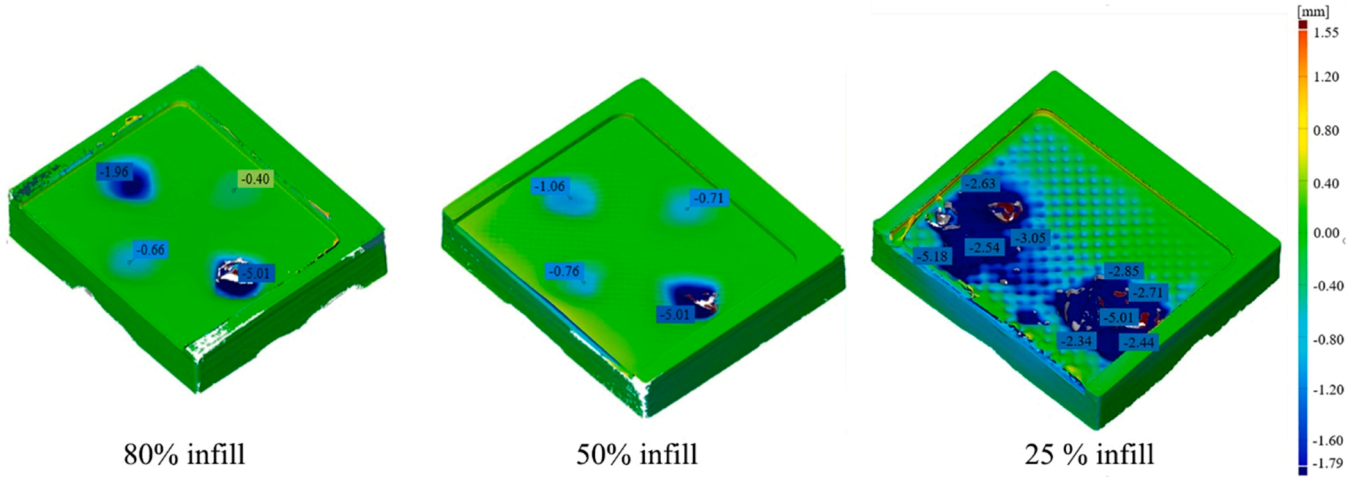

Fig. 12. Inserts after failure 80 %, 50 % and 25 % infill.

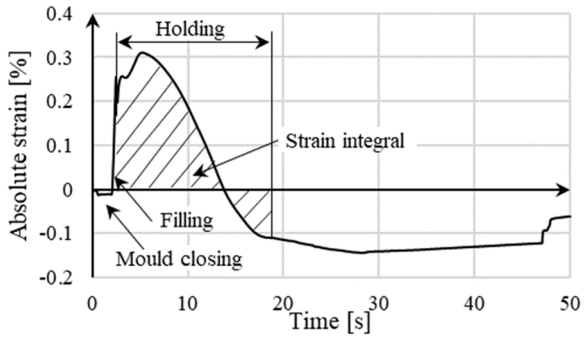

Fig. 13. Graphical interpretation of the strain integral.

respectively. In these equations, $c_1, c_2,$ are empirical constants. The c_1 and c_2 constants are mainly determined by the local geometry of the mould and the applied load. A good first estimate for m_0 is nominal product mass without compensation (holding pressure) and w_0 can be estimated by the thickness of the cooled product, which is the nominal dimension corrected by part shrinkage. A proper initial guess for the m_0 and w_0 parameters can be made based upon the CAD model of the injection moulded part. Naturally, all parameters can be determined most accurately with a series of injection moulding experiments and curve fitting. After the parameters are set properly, the expressions can predict product mass and local thickness with adequate accuracy.

$$m_{product} \approx c_1 \bullet \int_{t=start\ of\ holding}^{t=end\ of\ holding} \epsilon_{abs}(t)dt + m_0 \tag{2}$$

$$w_{product} \approx c_2 \bullet \int_{t=start\ of\ holding}^{t=end\ of\ holding} \epsilon_{abs}(t)dt + w_0 \tag{3}$$

The constants for linear fitting are presented in Table 3. The first values in each cell correspond to the NG linear fitting and the second to the FFG linear fitting. Nominal product mass (assuming a PP density of 900 kg/m^3) is 6.3 g and nominal product thickness is 2 mm (PP typically has a mould shrinkage of 1–2.5 %). The actual injection moulded products have lower thickness (approximately 1.8 mm in the constant 75-bar holding pressure section), which was already presented in Section 3.4. Assuming this w_0 thickness, the calculated product mass is 5.77 g, which is close to the m_0 values presented in Table 3. The fitted m_0 and w_0 constants show that the nominal values give a reasonable first estimate, which can be later refined.

Based on these correlations, strain measurement can be an adequate product quality monitoring tool. If an injection mould is fitted with a strain measurement system, the absolute strain integrals can be

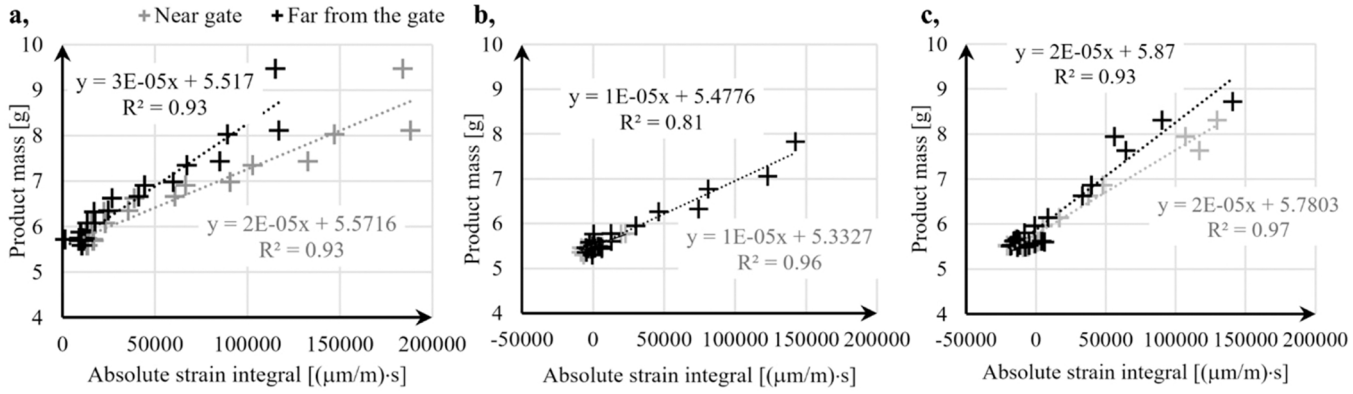

Fig. 14. Correlational diagrams between the strain integral and product mass for different infill levels: 80 % a), 50 % b) and 25 % c).

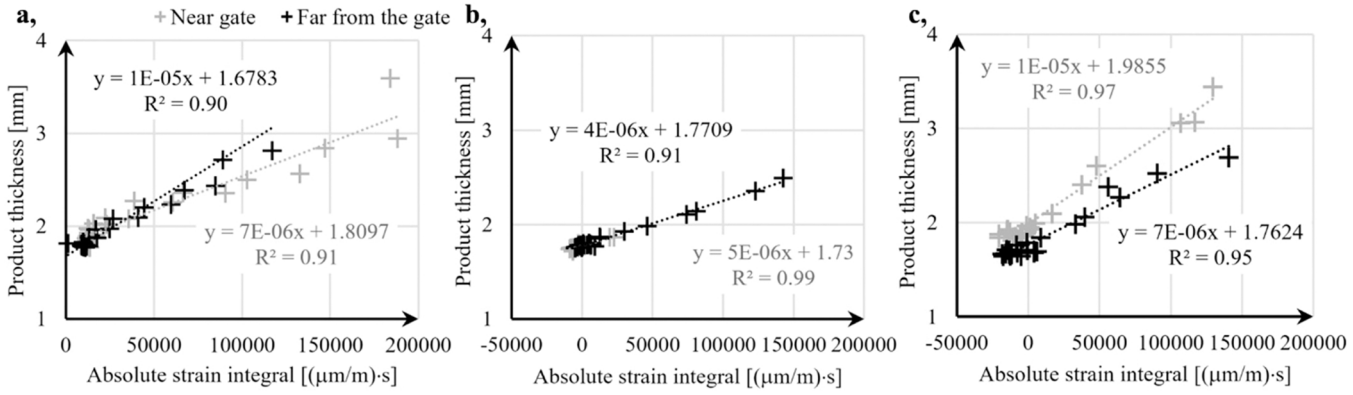

Fig. 15. Correlational diagrams between the strain integrals and product thicknesses for the different infill levels: 80 % a), 50 % b) and 25 % c).

Table 3
Constants for linear correlation between absolute strain integrals and product mass and thickness. The first values in each cell correspond to the fitting for the NG strains, and the second values to the FFG strains.

Infill percentage	c_1 (g/s)	m_0 [g]	c_2 (mm/s)	w_0 [mm]
80 %	$2 \bullet 10^{-5}/3 \bullet 10^{-5}$	5.57/5.52	$7 \bullet 10^{-6}/1 \bullet 10^{-5}$	1.81/1.68
50 %	$1 \bullet 10^{-5}/1 \bullet 10^{-5}$	5.48/5.33	$4 \bullet 10^{-6}/5 \bullet 10^{-6}$	1.77/1.73
25 %	$2 \bullet 10^{-5}/2 \bullet 10^{-5}$	5.78/5.87	$1 \bullet 10^{-5}/7 \bullet 10^{-6}$	1.99/1.76

automatically calculated based on the injection, the switchover and end of holding signals of the injection moulding machine. Simultaneous strain measurements at several locations can yield a more comprehensive picture of product quality. These automatically calculated integral values can then also be used to indicate unwanted deviations from nominal values during production in real time. With this automated product quality control, scrap can be minimized.

4. Summary

A comprehensive state monitoring method was applied for rapid-prototyped injection moulds. The measurement system can quantify operational strains, surface temperatures and volumetric temperatures of the additively manufactured mould inserts. The monitoring system also includes 3D scanning of the injection moulded products as well as mould inserts, both in their as-printed state and after their failure. The comprehensive state monitoring and quality analysis system is novel. In this research article, Material Extrusion AM technology was applied to produce mould inserts because of the wide availability, low cost and ease of use of this printing technology. An ABS filament (thermoplastic) was used for prototype mould making because of its high glass transition temperature and acceptable mechanical properties. Long delay times (~250 s) were also inserted between the cycles to protect the inserts from excessive heat loads.

The infill level of the printed inserts (80 %, 50 % and 25 %) were varied to examine the possibility of material saving and printing time reduction while monitoring the operational behaviour (strains, lifetime and temperature distribution) of the inserts. As infill level was reduced, the measured maximal operational strains increased from 0.13–0.15% of the 80 % infill insert at a constant 75-bar holding pressure, to 0.23–0.3 % in the case of the 50 % and 25 % infill inserts. The holding pressure where the inserts failed also dropped from 275 bar of the 80 % infill insert to 225 bar of the 25 % infill insert. The lifetime of the inserts decreased from 32 operational cycles of the 80 % infill insert to 24 cycles of the 25 % infill insert. Reduction of the infill level also results in the faster heating of the inserts because of the increasing volume percentage of air, which acts a thermal insulator. On the other hand, printing time was significantly reduced (from 4 h 1 min for the 80 % infill insert, to 2 h 48 min for the 25 % infill insert) and material requirement decreased.

The concept of strain integrals was also introduced, which is the definite integral of the measured absolute strain from the start of holding to the end of the holding phase. Correlational diagrams were set up between the absolute strain integrals and the measured product masses and thicknesses. A good linear correlation was found (mostly a correlational coefficient of $R^2 > 0.9$) between the integral and product properties. It means that the presented integral can be applied for product quality monitoring. This method can be more commonly applied in the future because if an injection mould is fitted with a strain measurement system, the strain integrals can be automatically calculated during production. These integrals then can signal the potential deviations in the mass and thickness of the injection moulded product with a strong correlation. Because of this, the findings of the present paper can pave the way for an in-line, automated product quality monitoring system once the strain measurement system is more commonly applied in injection moulds and it is properly integrated with the injection moulding machine.

In conclusion, Material Extrusion was found to be a suitable additive manufacturing technology for low-volume and prototype mould making and the variability of the infill percentage gives additional design freedom to engineers. Product size deviations from the nominal value were in acceptable range. The warpage and the shrinkage of the mould inserts should be considered and optimally compensated for prior to printing. For this, preliminary printing trials are needed to collect warpage and shrinkage data. If insert size and the shape deviations are compensated for properly, then low-volume moulds can be made in a single technological step. This is especially beneficial for the production of complex insert geometries, where conventional machining is lengthy and very costly due to the frequent tool changes and repositioning of the machined part.

Funding

This work was supported by the National Research, Development and Innovation Office, Hungary (OTKA FK134336, OTKA FK138501). Project no. RRF-2.3.1–21–2022–00009, titled National Laboratory for Renewable Energy has been implemented with the support provided by the Recovery and Resilience Facility of the European Union within the framework of Programme Széchenyi Plan Plus. The research was supported by the ÚNKP-22–3-II-BME-105 New National Excellence Program of the Ministry for Culture and Innovation from the source of the National Research, Development and Innovation Fund.

CRediT authorship contribution statement

Szabolcs Krizsma: Conceptualization, Methodology, Investigation, Data curation, Writing – original draft, Visualization. **András Suplicz:** Conceptualization, Formal analysis, Writing – review & editing, Supervision.

Declaration of Competing Interest

The authors declare that they have no known competing financial interests or personal relationships that could have appeared to influence the work reported in this paper.

Data Availability

Data will be made available on request.

Acknowledgements

The authors thank ARBURG HUNGÁRIA KFT. for the ARBURG Allrounder injection moulding machine, and TOOL-TEMP HUNGÁRIA KFT., LENZKES GMBH and PIOVAN HUNGARY KFT. for the accessories.

References

[1] G. Krizsma Sz, N.K. Kovács, J.G. Kovács, A. Suplicz, In-situ monitoring of deformation in rapid prototyped injection molds, Addit. Manuf. 42 (2021), https://doi.org/10.1016/j.addma.2021.102001, 102001/1-102001/8.
[2] N.H.M. Huzaim, S.Z.A. Rahim, L. Musa, A.E.-h Abdellah, M.M.A.B. Abdullah, A. Rennie, R. Rahman, S. Garus, K. Błoch, A.V. Sandu, P. Vizureanu, M. Nabiałek, Potential of rapid tooling in rapid heat cycle molding: a review, Materials 15 (2022) 3725, https://doi.org/10.3390/ma15103725.
[3] A.B. Lozano, S.H. Álvarez, C.V. Isaza, W. Montealegre-Rubio, Analysis and advances in additive manufacturing as a new technology to make polymer injection molds for world-class production systems, Polymers 14 (2022) 1646, https://doi.org/10.3390/polym14091646.
[4] Sz Krizsma, A. Suplicz, Comprehensive in-mould state monitoring of Material Jetting additively manufactured and machined aluminium injection moulds, J. Manuf. Process. 84 (2022) 1298–1309, https://doi.org/10.1016/j.jmapro.2022.10.070.
[5] B. Koker, R. Ruckdashel, H. Abajorga, N. Curcuru, M. Pugatch, R. Dunn, D. O. Kazmer, E.D. Wetzel, J.H. Park, Enhanced interlayer strength and thermal stability via dual material filament for material extrusion additive manufacturing, Addit. Manuf. 55 (2022), 102807, https://doi.org/10.1016/j.addma.2022.102807.
[6] D. Chantzis, X. Liu, D.J. Politis, Z. Shi, L. Wang, Design for additive manufacturing (DfAM) of hot stamping dies with improved cooling performance under cyclic loading conditions, Addit. Manuf. 37 (2021), 101720, https://doi.org/10.1016/j.addma.2020.101720.
[7] R. Muvunzi, D. Hagedorn-Hansen, S. Matope, X. Madyibi, C.B. Swart, M. Nagel, Industry case study: process chain for manufacturing of a large hybrid hot stamping tool with conformal cooling channels, Int. J. Adv. Manuf. Technol. 110 (2020) 1723–1730, https://doi.org/10.1007/s00170-020-05992-6.
[8] C.-C. Kuo, Z.-F. Jiang, X.-Y. Yang, S.-X. Chu, J.-Q. Wu, Characterization of a direct metal printed injection mold with different conformal cooling channels, Int. J. Adv. Manuf. Technol. 107 (2020) 1223–1238, https://doi.org/10.1007/s00170-020-05114-2.
[9] D. Török, B. Zink, T. Ageyeva, I. Hatos, M. Zobač, I. Fekete, R. Boros, H. Hargitai, J. G. Kovács, Laser powder bed fusion and casting for an advanced hybrid prototype mold, J. Manuf. Process. 81 (2022) 748–758, https://doi.org/10.1016/j.jmapro.2022.07.034.
[10] S.J. Park, J.H. Lee, J. Yang, W. Heogh, D. Kang, S.M. Yeon, S.H. Kim, S. Hong, Y. Son, J. Park, Lightweight injection mold using additively manufactured Ti-6Al-4V lattice structures, J. Manuf. Process. 79 (2022) 759–766, https://doi.org/10.1016/j.jmapro.2022.05.022.
[11] R. Mahshid, H.N. Hansen, K.L. Højbjerre, Strength analysis and modeling of cellular lattice structures manufactured using selective laser melting for tooling applications, Mater. Des. 104 (2016) 276–283, https://doi.org/10.1016/j.matdes.2016.05.020.
[12] M. Narvan, A. Ghasemi, E. Fereiduni, S. Kendrish, M. Elbestawi, Part deflection and residual stresses in laser powder bed fusion of H13 tool steel, Mater. Des. 204 (2021), 109659, https://doi.org/10.1016/j.matdes.2021.109659.
[13] W. Shan, H. Zhong, H. Mo, S. Zhao, P. Liu, Epoxy acrylate-based shape memory polymer via 3D printing, EXPRESS Polym. Lett. 15 (12) (2021) 1126–1134, https://doi.org/10.3144/expresspolymlett.2021.91.
[14] A. Bagalkot, D. Pons, D. Clucas, D. Symons, A methodology for setting the injection moulding process parameters for polymer rapid tooling inserts, Rapid Prototyp. J. (2019) 1493–1505, https://doi.org/10.1108/RPJ-10-2017-0217.
[15] L. Giorleo, B. Stampone, G. Trotta, Micro injection moulding process with high-temperature resistance resin insert produced with material jetting technology: Effect of part orientation, Addit. Manuf. 56 (2022), 102947, https://doi.org/10.1016/j.addma.2022.102947.
[16] B. Zink, N.K. Kovács, J.G. Kovács, Thermal analysis based method development for novel rapid tooling applications, Int. Commun. Heat Mass Transf. 108 (2019), 104297, https://doi.org/10.1016/j.icheatmasstransfer.2019.104297.
[17] E. Walsh, J.H. ter Horst, D. Markl, Development of 3D printed rapid tooling for micro-injection moulding, Chem. Eng. Sci. 235 (2021), 116498, https://doi.org/10.1016/j.ces.2021.116498.
[18] E. Walsh, N. Maclean, A. Turner, M. Alsuleman, E. Prasad, G. Halbert, J.H. ter Horst, D. Markl, Manufacture of tablets with structurally-controlled drug release using rapid tooling injection moulding, Int. J. Pharm. 624 (2022), 121956, https://doi.org/10.1016/j.ijpharm.2022.121956.
[19] M. Hopkins, S. Gunbaya, C. Hayes, V.F. Moritz, E. Fuenmayor, J.G. Lyons, D. M. Devine, Stereolithography (SLA) utilised to print injection mould tooling in order to evaluate thermal and mechanical properties of commercial polypropylene, Procedia Manuf. 55 (2021) 205–211, https://doi.org/10.1016/j.promfg.2021.10.029.
[20] G.A. Mendible, J.A. Rulander, S.P. Johnston, Comparative study of rapid and conventional tooling for plastics injection molding, Rapid Prototyp. J. 23 (2) (2017) 344–352, https://doi.org/10.1108/RPJ-01-2016-0013.
[21] G.G. Arias, F.J. Díaz, E.R. Ramirez, J.V. Guzman, Thermal analysis by finite elements of hotends for 3D printing by fused filament fabrication, Period. Polytech. Mech. Eng. 65 (2) (2021) 129–133, https://doi.org/10.3311/PPme.16203.
[22] C.-M. Choe, W.-C. Yang, U.-H. Kim, B.-G. Ri, M.-S. Om, Manufacture of centrifugal compressor impeller using FDM and investment casting, Int. J. Adv. Manuf. Technol. 118 (2022) 173–181, https://doi.org/10.1007/s00170-021-07894-7.
[23] A.M. Gohn, D. Brown, G. Mendis, S. Forster, N. Rudd, M. Giles, Mold inserts for injection molding prototype applications fabricated via material extrusion additive manufacturing, Addit. Manuf. 51 (2022), 102595, https://doi.org/10.1016/j.addma.2022.102595.

[24] S.J. Park, J.E. Lee, J. Park, N.-K. Lee, Y. Son, S.-H. Park, High-temperature 3D printing of polyetheretherketone products: perspective on industrial manufacturing applications of super engineering plastics, Mater. Des. 211 (2021), 110163, https://doi.org/10.1016/j.matdes.2021.110163.
[25] G. Singh, J.-M. Missiaen, D. Bouvard, J.-M. Chaix, Additive manufacturing of 17–4 PH steel using metal injection molding feedstock: analysis of 3D extrusion printing, debinding and sintering, Addit. Manuf. 47 (2021), 102287, https://doi.org/10.1016/j.addma.2021.102287.
[26] M. Seleznev, J.D. Roy-Mayhew, Bi-metal composite material for plastic injection molding tooling applications via fused filament fabrication process, Addit. Manuf. 48 (2021), 102375, https://doi.org/10.1016/j.addma.2021.102375.
[27] P. Yeole, S. Kim, A.A. Hassen, V. Kumar, V. Kunc, U. Vaidya, Large-scale additive manufacturing tooling for extrusion-compression molds, Addit. Manuf. Let. 1 (2021), 100007, https://doi.org/10.1016/j.addlet.2021.100007.
[28] E. Fuenmayor, C. O'Donnell, N. Gately, P. Doran, D.M. Devine, J.G. Lyons, C. McConville, I. Major, Mass-customization of oral tablets via the combination of 3D printing and injection molding, Int. J. Pharm. 569 (2019), 118611, https://doi.org/10.1016/j.ijpharm.2019.118611.
[29] R. Wick-Joliat, M. Tschamper, R. Kontic, D. Penner, Water-soluble sacrificial 3D printed molds for fast prototyping in ceramic injection molding, Addit. Manuf. 48 (2021), 102408, https://doi.org/10.1016/j.addma.2021.102408.
[30] P. Minetola, F. Calignano, M. Galati, Comparing geometric tolerance capabilities of additive manufacturing systems for polymers, Addit. Manuf. 32 (2020), 101103, https://doi.org/10.1016/j.addma.2020.101103.